EAM-based high-speed 100-km OFDM transmission featuring tolerant modulator operation enabled using SSII cancellation

Hsing-Yu Chen,[1,3] Chia-Chien Wei,[2,*] I-Cheng Lu,[1] Yu-Chao Chen,[1] Hsuan-Hao Chu,[1] and Jyehong Chen[1]

[1]*Department of Photonics, National Chiao-Tung University, Hsinchu 300 Taiwan*
[2]*Department of Photonics, National Sun Yat-sen University, Kaohsiung 804 Taiwan*
[3]*Information and Communications Research Labs, Industrial Technology Research Institute, Hsinchu 310, Taiwan*
[*]*ccwei@mail.nsysu.edu.tw*

Abstract: In this study, a technique was developed to compensate for nonlinear distortion through cancelling subcarrier-to-subcarrier intermixing interference (SSII) in an electroabsorption modulator (EAM)-based orthogonal frequency-division multiplexing (OFDM) transmission system. The nonlinear distortion to be compensated for is induced by both EAM nonlinearity and fiber dispersion. Because an OFDM signal features an inherently high peak-to-average power ratio, a trade-off exists between the optical modulation index (OMI) and modulator nonlinearity. Therefore, the nonlinear distortion limits the operational tolerance of the bias voltage and the driving power to a small region. After applying the proposed SSII cancellation, the OMI of an OFDM signal was increased yielding only a small increment of nonlinear distortion, and the tolerance region of the operational conditions was also increased. By employing the proposed scheme, this study successfully demonstrates 50-Gbps OFDM transmission over 100-km dispersion-uncompensated single-mode fiber based on a single 10-GHz EAM.

OCIS codes: (060.2330) Fiber optics communications; (060.0060) Fiber optics and optical communications.

References and links

1. T. Koonen, "Fiber to the home/fiber to the premises: what, where, and when?" Proc. IEEE **94**(5), 911–934 (2006).
2. P. D. Townsend, G. Talli, C. W. Chow, E. M. MacHale, C. Antony, R. Davey, T. De Ridder, X. Z. Qiu, P. Ossieur, H. G. Krimmel, D. W. Smith, I. Lealman, A. Poustie, S. Randel, and H. Rohde, "Long reach passive optical networks" in Proc. of LEOS, ThW1 (2007).
3. R. P. Davey, D. B. Grossman, M. Rasztovits-Wiech, D. B. Payne, D. Nesset, A. E. Kelly, A. Rafel, S. Appathurai, and S. H. Yang, "Long-reach passive optical networks," J. Lightwave Technol. **27**(3), 273–291 (2009).
4. K. Y. Cho, K. Tanaka, T. Sano, S. P. Jung, J. H. Chang, Y. Takushima, A. Agata, Y. Horiuchi, M. Suzuki, and Y. C. Chung, "Long-reach coherent WDM PON employing self-polarization-stabilization technique," J. Lightwave Technol. **29**(4), 456–462 (2011).
5. D. Shea and J. Mitchell, "A 10 Gb/s 1024-way-split 100-km long-reach optical-access network," J. Lightwave Technol. **25**(3), 685–693 (2007).
6. D. Z. Hsu, C. C. Wei, H. Y. Chen, J. Chen, M. C. Yuang, S. H. Lin, and W. Y. Li, "21 Gb/s after 100 km OFDM long-reach PON transmission using a cost-effective electro-absorption modulator," Opt. Express **18**(26), 27758–27763 (2010).
7. D. Z. Hsu, C. C. Wei, H. Y. Chen, W. Y. Li, and J. Chen, "Cost-effective 33-Gbps intensity modulation direct detection multi-band OFDM LR-PON system employing a 10-GHz-based transceiver," Opt. Express **19**(18), 17546–17556 (2011).
8. D. Z. Hsu, C. C. Wei, H. Y. Chen, Y. C. Lu, and J. Chen, "A 40-Gbps OFDM LR-PON system over 100-km fiber employing an economical 10-GHz-based transceiver" in Proc. of OFC, OW4B.2 (2012).

#208894 - $15.00 USD Received 25 Mar 2014; revised 19 May 2014; accepted 20 May 2014; published 6 Jun 2014

9. A. Gharba, P. Chanclou, M. Ouzzif, J. L. Masson, L. A. Neto, R. Xia, N. Genay, B. Charbonnier, M. Hélard, E. Grard, and V. Rodrigues, "Optical transmission performance for DML considering laser chirp and fiber dispersion using AMOOFDM" in Proc. of ICUMT, 1022–1026 (2010).
10. D.-Z. Hsu, C.-C. Wei, H.-Y. Chen, Y.-C. Lu, C.-Y. Song, C.-C. Yang, and J. Chen, "SSII cancellation in an EAM-based OFDM-IMDD transmission system employing a novel dynamic chirp model," Opt. Express **21**(1), 533–543 (2013).
11. C. C. Wei, "Small-signal analysis of OOFDM signal transmission with directly modulated laser and direct detection," Opt. Lett. **36**(2), 151–153 (2011).
12. C. C. Wei, "Analysis and iterative equalization of transient and adiabatic chirp effects in DML-based OFDM transmission systems," Opt. Express **20**(23), 25774–25789 (2012).
13. W. Yan, B. Liu, L. Li, Z. Tao, T. Takahara, and J. C. Rasmussen, "Nonlinear Distortion and DSP-based Compensation in Metro and Access Networks using Discrete Multi-tone" in Proc. of ECOC, Mo.1.B.2. (2012)
14. T. Alves, J. Morgado, and A. Cartaxo, "Linearity improvement of directly modulated PONs by digital predistortion of coexisting OFDM-based signals" in Proc. of ANIC, AW4A.2. (2012)
15. Y. Bao, Z. Li, J. Li, X. Feng, B. O. Guan, and G. Li, "Nonlinearity mitigation for high-speed optical OFDM transmitters using digital pre-distortion," Opt. Express **21**(6), 7354–7361 (2013).
16. H. Y. Chen, C. C. Wei, Y. C. Chen, H. H. Chu, C.Y. Song, I. C. Lu, and J. Chen, "50-Gbps 100-km EAM-based OFDM-IMDD Transmission Employing Novel SSII Cancellation" (submitted) (2014).
17. B. Liu, J. Shim, Y.-J. Chiu, H. F. Chou, J. Piprek, and J. E. Bowers, "Slope Efficiency and Dynamic Range of Traveling-Wave Multiple-Quantum-Well Electroabsorption Modulators," IEEE Photon. Technol. Lett. **16**(2), 590–592 (2004).
18. W.-R. Peng, X. Wu, V. R. Arbab, K.-M. Feng, B. Shamee, L. C. Christen, J.-Y. Yang, A. E. Willner, and S. Chi, "Theoretical and Experimental Investigations of Direct-Detected RF-Tone-Assisted Optical OFDM Systems," J. Lightwave Technol. **27**(10), 1332–1339 (2009).
19. T. N. Duong, N. Genay, M. Ouzzif, J. Le Masson, B. Charbonnier, P. Chanclou, and J. C. Simon, "Adaptive Loading Algorithm Implemented in AMOOFDM for NG-PON System Integrating Cost-Effective and Low-Bandwidth Optical Devices," IEEE Photon. Technol. Lett. **21**(12), 790–792 (2009).

1. Introduction

To decrease capital and operational expenditures by means of consolidating the O/E/O conversion interfaces inside existing networks, an optically amplified large-split long-reach passive optical network (LR-PON) has been proposed to integrate access networks and metro networks [1–5]. However, to ensure that the system remains cost-effective, the optical intensity modulation and direct-detection (IMDD) scheme remains preferred, because it uses commercially available and inexpensive transceivers [5–8] such as 10-GHz-class electroabsorption modulators (EAMs) and PIN receivers. To support data rates higher than 40 Gbps and provide a reach extending to 100 km over a single wavelength, orthogonal frequency-division multiplexing (OFDM) transmission combined with high spectral-efficiency quadrature amplitude modulation (QAM) format has emerged as one of the most promising candidates. Because dispersion induces power fading in an IMDD system, another major benefit of employing OFDM in such systems is the flexible allocation of subcarriers to efficiently use the available bandwidth [5–10]. Moreover, dispersion-induced nonlinear distortion is another major obstacle that must be overcome in optical OFDM-IMDD systems. The distortion has been investigated theoretically and experimentally in the form of subcarrier-to-subcarrier intermixing interference (SSII) [7,10–13], and an SSII cancellation scheme has been proposed to eliminate the nonlinear distortion [10,11]. As an alternative approach, nonlinear Volterra filtering has been proposed to compensate for the dispersion-induced distortion [13]. Furthermore, because an OFDM signal features an inherently high peak-to-average power ratio and the transfer curve of an EAM exhibits a limited linear region, the optical modulation index (OMI) is typically maintained at a small value to avoid severe nonlinear distortion. To combat modulator nonlinearity, numerous predistortion schemes to linearize optical transmitters have been proposed [14,15]. However, in these schemes, only modulator nonlinearity is compensated for and dispersion-induced distortion is not considered; thus, the transmission performance level is degraded by dispersion-induced distortion. When the nonlinear transfer curve of an EAM is modeled as a second-order expression, the EAM nonlinearity can be combined with the SSII model [16], and both the

#208894 - $15.00 USD Received 25 Mar 2014; revised 19 May 2014; accepted 20 May 2014; published 6 Jun 2014

nonlinearity of the EAM and dispersion-induced distortion can be concurrently compensated for by employing the SSII cancellation technique.

To optimize the performance level of 10-GHz EAM-based OFDM transmission, in this study, SSII cancellation was used to eliminate both EAM nonlinearity and dispersion-induced distortion. Because both the chirp parameters and the modulation linearity of an EAM vary based on the bias voltage, increased EAM nonlinearity is typically the cost of attaining a negative chirp and elevated OMI. When the proposed SSII cancellation method is employed, the control of the bias voltage and the driving power of an EAM used for adjusting the OMI and the chirp-related bandwidth could be less sensitive to EAM nonlinearity and dispersion-induced distortion. Therefore, various operational conditions featuring distinct bias voltages and driving powers were applied to investigate transmission performance level with and without the use of the proposed SSII cancellation method. The experimental results demonstrate that the modulator operational tolerance of both bias voltage and driving power can be improved. For instance, to achieve 43.5-Gbps 100-km transmission (i.e., 40-Gbps data capacity, an overhead of 7% FEC coding, and 1.5% cyclic prefix (CP)) by using the proposed scheme, the bias-voltage and driving-power tolerance can be increased from approximately 0.1 V and 2 dB to > 0.4 V and > 5 dB, respectively. Moreover, when SSII cancellation is applied, optimizing the modulator operation can result in an increase in OMI and available bandwidth, thereby improving the maximal capacity by 12.5% to achieve 50-Gbps transmission over a 100-km dispersion-uncompensated fiber.

2. Theory of SSII and the SSII cancellation technique

The dispersion-induced distortion of a chirped OFDM signal has been approximated as an SSII using a second-order small-signal model [10–12]. The non-constant chirp parameter was considered in the model to precisely estimate the chirp-related nonlinear distortion [10]. An underlying assumption of the model was a linear intensity modulation: the modulation slope was constant, but a practical EAM showed a deceasing modulation slope with increasing reverse bias (for example [6,17],), which resulted in nonlinear intensity modulation. Thus, EAM nonlinearity cannot be neglected, particularly when the OMI is increased. To extend the second-order small-signal model to include EAM nonlinearity, the transfer curve of an EAM is considered as a power series in the modulation voltage. When only the second-order nonlinearity is considered for the sake of simplicity, the normalized optical power can be approximated as $P \cong 1 + X + p_2 X^2$, where $X = \Sigma_{n=1}^{N} \Re\{x_n e^{jn\omega t}\}$ is the normalized driving signal, N is the subcarrier number, $\omega/(2\pi)$ is the subcarrier spacing, x_n is normalized data symbol of the n^{th} subcarrier at the output of an EAM, and p_2 is the weighting of the second-order nonlinear distortion induced by an EAM, in contrast to $P \cong 1 + X$ in [10]. The non-constant chirp parameter is set as $\alpha \cong \alpha_0 + \alpha_1 X$ [10]. Thus, the normalized envelope of the chirped optical field, $E = \sqrt{P}\exp(-j(\alpha \ln P)/2)$, can be approximated as follows:

$$E \cong 1 + \frac{1 - j\alpha_0}{2} X - \frac{\left(1 + \alpha_0^2 - 4p_2\right) + j4\left(\alpha_1 + \alpha_0 p_2\right)}{8} X^2, \qquad (1)$$

where X^2 is the second-order term, and the higher-order terms of x_n are neglected. When only chromatic dispersion is considered, the response of fiber transmission is $\exp(jn^2\theta_D)$ for the n^{th} subcarrier, where θ_D is defined as $\omega^2\beta_2 L/2$, and L and β_2 are the fiber length and dispersion parameter, respectively. Thus, if $\Theta\{\cdot\}$ represents the effect of dispersive transmission, it follows, for instance, that $\Theta\{X\} = \Sigma_{n=1}^{N} \Re\{x_n e^{jn\omega t}\} \cdot e^{jn^2\theta_D}$. After square-law

#208894 - $15.00 USD Received 25 Mar 2014; revised 19 May 2014; accepted 20 May 2014; published 6 Jun 2014

photo-detection and second-order approximation are conducted, the normalized received signal is as follows:

$$R = \left|\Theta\{E\}\right|^2 \cong 1 + \Re\{(1 - j\alpha_0)\Theta\{X\}\} + \underbrace{\frac{(1+\alpha_0^2)}{4} \times \left[\left|\Theta\{X\}\right|^2 - \left|\sec\theta_p\right| \cdot \Re\left\{\Theta\left\{X^2\right\} e^{j\theta_p}\right\} + u\left|\sec\theta_p\right| \cdot \Re\left\{\Theta\left\{X^2\right\} e^{j\theta_p}\right\}\right]}_{SSII}, \quad (2)$$

where $\theta_p \equiv \tan^{-1}(4(\alpha_1 + \alpha_0 p_2)/(1 + \alpha_0^2 - 4p_2))$ and $u = 4p_2/(1+\alpha_0^2)$. The second term at the right hand side of R corresponds to the desired OFDM signal, and the third term is composed of the intermixing terms among subcarriers. The combination of the second-order terms is the modified SSII, including the nonlinear distortion induced by an EAM. Moreover, at an optical back-to-back (BtB, $L = 0$), the SSII is converted to $p_2 X^2$, which becomes 0 when EAM nonlinearity is not considered. Thus, the SSII caused by EAM nonlinearity typically localizes at the baseband [18] and degrades the subcarriers at low frequencies. By contrast, the dispersion-induced SSII degrades the subcarriers at high frequencies, which are more strongly affected by dispersion compared with low frequencies.

To mitigate the influence of nonlinear distortion, an SSII cancellation technique was developed for use at the receiver; the block diagram is shown in Fig. 1 [10,12], with the schematic plot of the SSII spectra, which illustrate the difference between two nonlinear distortions. In this approach, the received OFDM data featuring the nonlinear distortion are demodulated and detected as the regular OFDM demodulation process. The detected data are used as X to calculate the SSII based on the SSII model and Eq. (2), and the required parameters and responses are estimated using training symbols, which is detailed in [10]. The calculated SSII is then fed back to perform the SSII cancellation, and the OFDM data obtained after the SSII cancellation are demodulated again to increase the amount of accurate data detected.

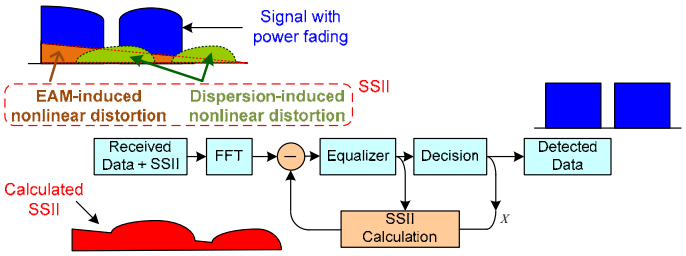

Fig. 1. The block diagram of the SSII cancellation technique and the schematic spectra of SSII.

3. Experimental setup and results

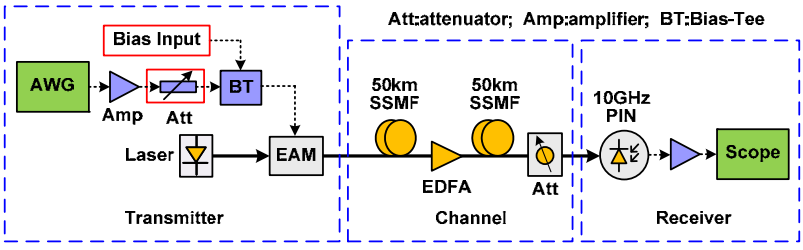

Fig. 2. Experimental setup of an EAM-based OFDM-IMDD 100-km transmission.

The experimental setup used in this study is shown in Fig. 2. The baseband electrical OFDM signal was generated by an arbitrary waveform generator (AWG, Tektronix® AWG70002A),

#208894 - $15.00 USD Received 25 Mar 2014; revised 19 May 2014; accepted 20 May 2014; published 6 Jun 2014

featuring a 50-GS/s sampling rate and 8-bit resolution. The driving signal consisted of a 16-QAM OFDM signal that had an FFT size of 1024 and a CP of 16, and the data were encoded at 2nd–206th subcarriers featuring a bandwidth of 10 GHz. An electrical attenuator, which was preceded by an electrical amplifier, was inserted to adjust the driving power of the EAM (CIP 10G-LR-EAM-1550). After EAM-based intensity modulation and 100-km standard single-mode fiber (SSMF) transmission with an inline EDFA inserted, the signal was direct-detected using a 10-GHz PIN receiver and captured using a digital oscilloscope (Tektronix® DPO 71604) that had a 50-GS/s sampling rate and a 3-dB bandwidth of 16 GHz. The captured digital signal was demodulated using an offline DSP program, which included the SSII cancellation technique. Last, the signal-to-noise ratio (SNR) was measured and the number of errors was determined to calculate the bit error rate (BER).

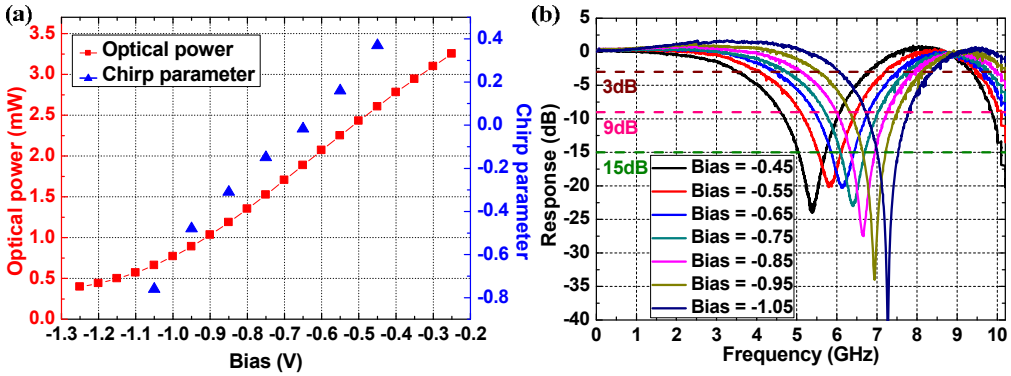

Fig. 3. (a) The transfer curve of the EAM and the corresponding chirp parameters, and (b) the 100-km SSMF channel response with different bias voltages.

Table 1. Chirp Parameters and 3-dB, 9-dB, and 15-dB Bandwidth within 10 GHz at Different Biases

Bias (V)	-0.45	-0.55	-0.65	-0.75	-0.85	-0.95	-1.05
Chirp parameter	0.37	0.16	–0.017	–0.15	–0.31	–0.48	–0.76
3-dB bandwidth (GHz)	6.1	6.36	6.56	6.78	7.14	7.42	7.67
9-dB bandwidth (GHz)	8.38	8.64	8.65	8.68	8.73	8.84	8.93
15-dB bandwidth (GHz)	9.32	9.41	9.43	9.39	9.4	9.43	9.47

Figure 3(a) presents the measured transfer curve of the EAM and the corresponding chirp parameters. The results show that the linear operational bias was approximately –0.55 V and the chirp parameter decreased when the bias was lowered. Figure 3(b) shows the frequency response of the 100-km SSMF transmission at EAM bias voltages ranging from –0.45 to –1.05 V. The chirp parameter was calculated based on the notch point of the frequency response [5]; Table 1 lists the corresponding 3-dB, 9-dB, and 15-dB bandwidths within 10 GHz. Lowering the bias voltage can increase the negativity of the chirp parameter and widen the bandwidth; for example, the 3-dB bandwidth was enhanced by 17% when the bias was lowered from –0.55 to –0.95 V. Critically, lowering the bias voltage can widen the bandwidth of the baseband, where a digital-analog-converter (DAC) can generate subcarriers of enhanced electrical SNR, and thus the OFDM signal can carry increased amounts of information. However, the transfer curve depicted in Fig. 3(a) indicates that the low bias voltages undergo more nonlinear distortions than do the high bias voltages. The other key factor in optimizing performance is the OMI. Although, the OMI can be increased by lowering bias voltage and/or increasing driving power, a large OMI can increase the modulation nonlinearity to cause signal clipping. Therefore, increasing the OMI must be balanced against signal clipping. In this work, the bias voltages between –1.05 and –0.45 V

#208894 - $15.00 USD Received 25 Mar 2014; revised 19 May 2014; accepted 20 May 2014; published 6 Jun 2014

and driving powers between −1.57 and −8.97 dBm were used to investigate signal performance.

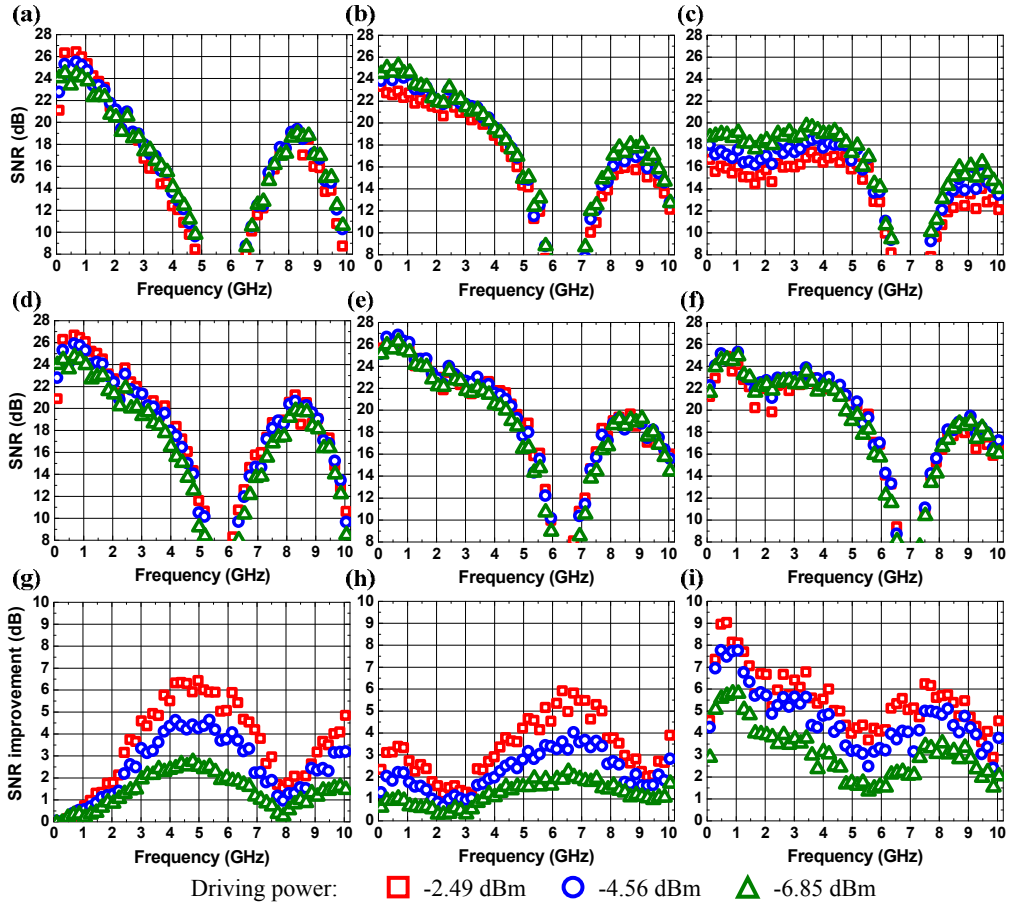

Fig. 4. The SNR without SSII cancellation at the bias (a) −0.55 V, (b) −0.75 V and (c) −0.95 V, and the SNR with SSII cancellation at the bias of (d) −0.55 V, (e) −0.75 V and (f) −0.95 V, and the corresponding SNR improvement at the bias of (g) −0.55 V, (h) −0.75 V and (i) −0.95 V.

Figures 4(a), (b), and (c) show the SNR of each OFDM subcarrier at the received power of −6 dBm and bias voltages of −0.55, −0.75, and −0.95 V, respectively, at the selected driving powers of −2.49, −4.56, and −6.85 dBm. The results show that the SNR at frequencies less than approximately 3 GHz increasingly degraded when the bias was changed from −0.55 to −0.95 V; the degradation was primarily caused by modulator nonlinearity, which is in contrast to the degradation at high frequencies that is caused by dispersion-induced distortion. After applying SSII cancellation, the corresponding SNR values of the distinct biases were calculated, which are shown in Figs. 4(d)-(f). By using the proposed technique, nonlinear distortion was reduced; however, because only second-order distortion was eliminated, highly nonlinear cases, such as the one with low bias shown in Fig. 4(f), might still underperform compared with other cases that are less nonlinear. The SNR improvement originating from the SSII cancellation is shown in Figs. 4(g)-(i), in which higher SNR improvements indicate greater SSII compensation. These results demonstrate that both types of distortion can be cancelled by using SSII cancellation: at the bias voltage of −0.55 V (Fig. 4(g)), the major improvement originated from the cancellation of the dispersion-induced distortion located at

#208894 - $15.00 USD Received 25 Mar 2014; revised 19 May 2014; accepted 20 May 2014; published 6 Jun 2014

high frequencies; by contrast, because EAM nonlinearity was severe at the bias voltage of −0.95 V, the SNR was improved the most at low frequencies (Fig. 4(i)). Moreover, because increasing the driving power increased the nonlinear distortion, the improvement in SNR was enhanced following SSII cancellation, as shown in Figs. 4(g)-(i). However, as a result of the trade-off between the OMI and (residual) nonlinear distortion, the SNR did not monotonically change with the driving power, as shown in Figs. 4(a)-(f).

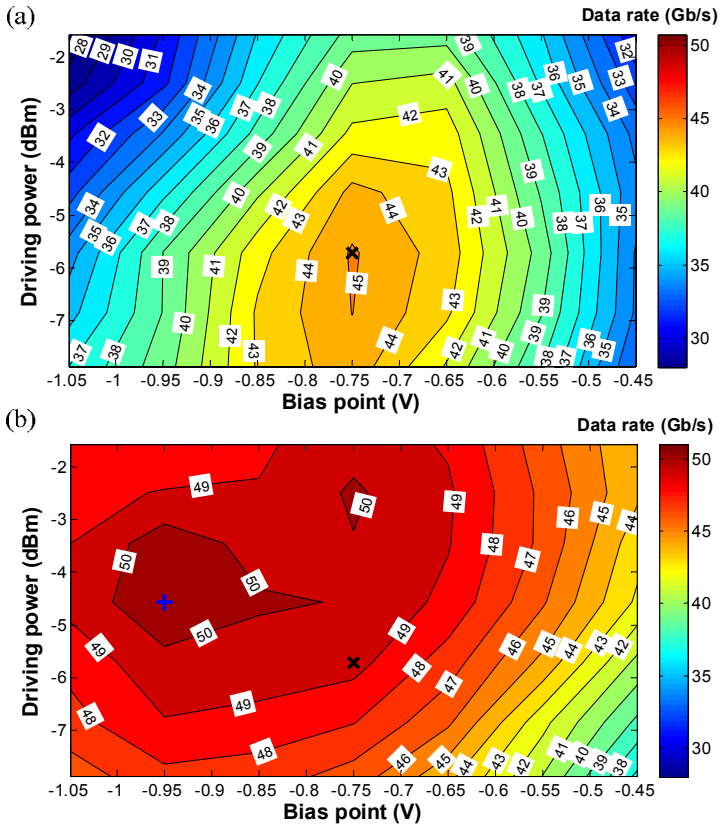

Fig. 5. Estimated data rate after 100-km SSMF transmission as the function of driving power of the EAM and bias voltage (a) without and (b) with SSII cancellation.

Because power fading and (residual) nonlinear distortion depend on the frequency, evaluating transmission performance under distinct operational conditions by using the measured SNR can be challenging (Fig. 4). To examine transmission performance in a simple manner, the SNRs of multiple subcarriers can be transformed into a single parameter: the maximal achievable data rate. Thus, by applying the bit-loading algorithm [19] together with the required BER of 3.8×10^{-3} (the FEC limit) to the measured SNRs of the OFDM signals, the maximal data rates of −6-dBm OFDM signals were estimated at various bias voltages and distinct driving powers of the EAM. The estimated data rates obtained before and after applying the SSII cancellation are shown in Figs. 5(a) and (b), respectively. Because the nonlinearity of an EAM rapidly increases when the bias voltage is lowered below −0.75 V, the data rate in Fig. 5(a) does not increase with the increased bandwidth that is provided by the more negative chirp occurring at low bias voltages compared with high biases. Moreover, a driving power of −5.7 dBm was the optimal trade-off between OMI and nonlinearity, and the corresponding maximal capacity was 45.12 Gbps. After applying SSII cancellation to reduce nonlinearity (Fig. 5(b)), the optimal operational condition was achieved by reducing

#208894 - $15.00 USD Received 25 Mar 2014; revised 19 May 2014; accepted 20 May 2014; published 6 Jun 2014

bias voltage to gain more transmission bandwidth and enhancing the driving power to increase the OMI, and therefore, the maximal data rate was increased to > 50 Gbps. Moreover, comparison with the results in Fig. 5(a) indicates that applying the proposed SSII cancellation also caused the data rate to become tolerant to operational conditions. For example, to achieve < 2-Gbps variation in the data rate (i.e., the data rates of > 43 and > 48 Gbps in Figs. 5(a) and (b), respectively), the eligible operational area shown in Fig. 5(b) is considerably larger than that shown in Fig. 5(a). As another example, to achieve a data rate of 43.5 Gbps after 100-km transmission (i.e., 40-Gbps data capacity, an overhead of 7% FEC coding, and 1.5% CP) by using the proposed scheme, the bias-voltage and driving-power tolerance can be increased from approximately 0.1 V and 2 dB to > 0.4 V and >5 dB, respectively. In fact, according to the discussion of the effects on decreasing the nonlinear distortion employing the SSII cancellation, the tolerance of the operational conditions could be enhanced even at different fiber distances longer or shorter than 100 km for different network applications. Figures 6(a) and (b) show the highest data rates and corresponding driving powers required at various bias voltages, respectively. By using SSII cancellation, the maximal data rate was increased by 12.5%, from 45.12 to 50.78 Gbps, and the smoothness of the data-rate variation with voltage bias was clearly enhanced. Furthermore, the optimal bias was lowered and the required driving powers were increased when SSII cancellation was applied, as shown in Figs. 6(a) and (b), respectively, indicating that the OMI was increased and thus performance and capacity were enhanced.

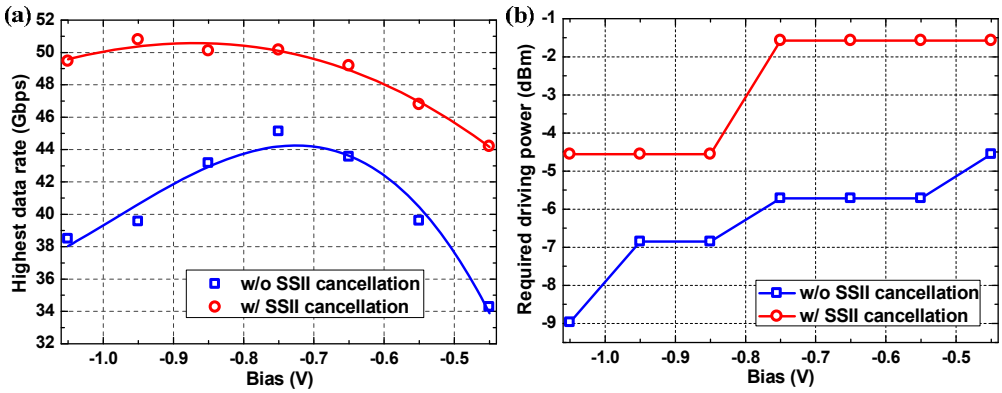

Fig. 6. (a) Highest data rate and (b) the corresponding driving powers required to reach the highest data rate at different bias voltage.

To confirm the estimated data rate shown in Figs. 5 and 6, the selected bias voltages were used to verify the experimental results of the bit-loading algorithm. The respective optimized driving powers shown in Fig. 6(b) were used, and Figs. 7(a), (b) and (c) show the SNR of each OFDM subcarrier obtained, with and without applying the bit-loading algorithm, at bias voltages of –0.55, –0.75, and –0.95 V, respectively; the corresponding results obtained after applying SSII cancellation are plotted in Figs. 7(d), (e) and (f), respectively. The bit numbers of these six bit-loading results are shown in Figs. 7(g)-(i). The increment in bit number after applying the SSII cancellation can be clearly observed, and it corresponds to the SNR improvement shown in Figs. 4(g)-(i). In Fig. 7(g), the modulator nonlinearity at the bias voltage of –0.55 V is relatively small, due to the cancellation of the major distortion induced by dispersion, the subcarriers located at high frequencies show more increment in bit number. By contrast, because EAM nonlinearity became a major effect at the bias voltage of –0.95 V in Fig. 7(i), the most increment in bit number was at low frequencies. The measured BERs in the results shown in Figs. 7(a), (b), (c), (d), (e) and (f) were 1.6×10^{-3}, 1.8×10^{-3}, 3.1×10^{-3}, 1.2×10^{-3}, 1.9×10^{-3}, and 3.4×10^{-3}, respectively; all of these BERs were lower than the required FEC limit, confirming the estimated results in Figs. 5 and 6. The results shown in

#208894 - $15.00 USD Received 25 Mar 2014; revised 19 May 2014; accepted 20 May 2014; published 6 Jun 2014

Fig. 7(f) demonstrate that a 50.78-Gbps signal was successfully transmitted over a 100-km SSMF by using the SSII cancellation technique.

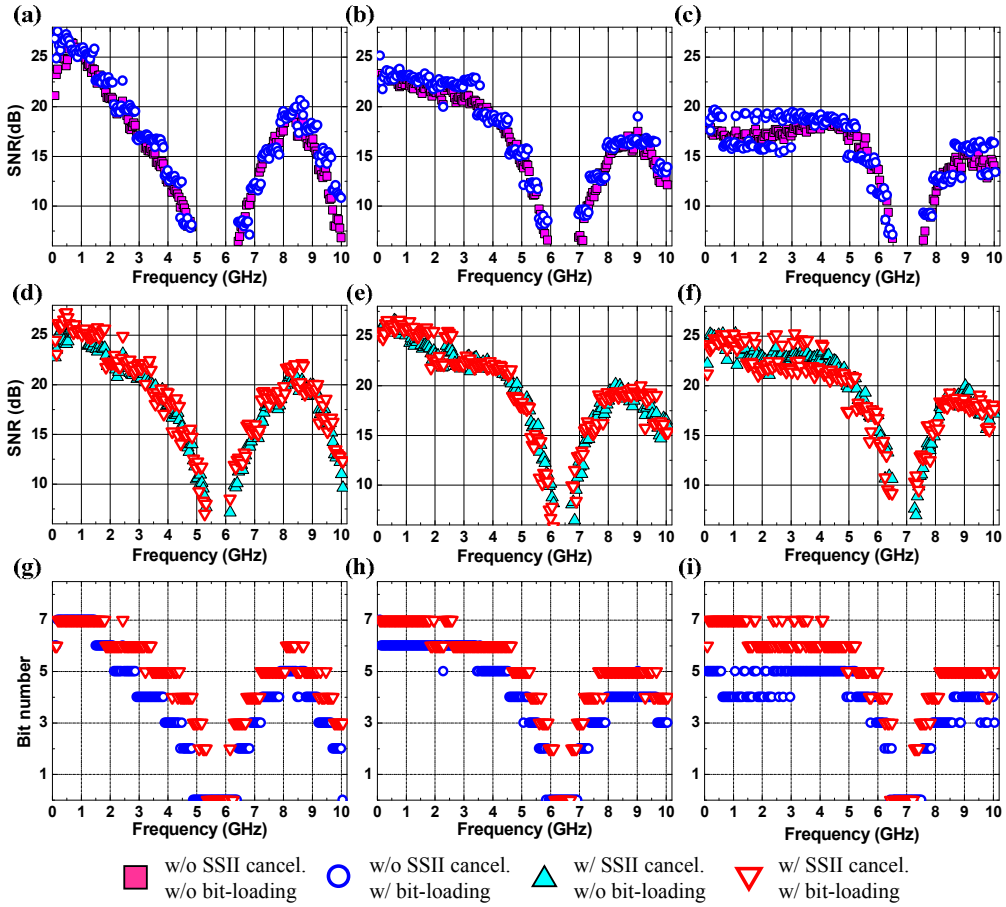

Fig. 7. The SNR without SSII cancellation before and after applying the bit-loading algorithm at the bias of (a) −0.55 V, (b) −0.75 V and (c) −0.95 V, the SNR with SSII cancellation at the bias of (d) −0.55 V, (e) −0.75V and (f) −0.95 V, and the corresponding bit numbers after applying bit-loading at the bias of (g) −0.55 V, (h) −0.75 V and (i) −0.95 V.

4. Conclusion

This paper describes nonlinear-distortion compensation that is achieved by employing an SSII-cancellation technique proposed for use in EAM-based OFDM-IMDD transmission systems. By using this technique, the nonlinear distortion induced by both EAM nonlinearity and fiber dispersion can be concurrently eliminated and, consequently, the OMI can be increased to optimize the system. Moreover, the tolerance regions of the operational conditions, which include the bias voltage and driving power of the EAM, are increased after applying the SSII-cancellation technique. The experimental results indicate that by using the technique, the data rate is enhanced by 12.5%, generating an improved, 50-Gbps 100-km EAM-based OFDM-IMDD system.

#208894 - $15.00 USD Received 25 Mar 2014; revised 19 May 2014; accepted 20 May 2014; published 6 Jun 2014